T.4: Studies on electromagnetically induced transparency in ^{87}Rb atoms

Charu Mishra
Laser Physics Applications Section
Email: charu.physics91@gmail.com

Abstract
The electromagnetically induced transparency (EIT) is a consequence of the quantum interference effect, which gives rise to sub-natural line-width. This trait of EIT finds applications in precision spectroscopy, precise atomic clocks [1], high resolution spectroscopy [2], and laser locking [3]. In this article, the EIT is studied experimentally and theoretically in D_2 line transition of ^{87}Rb atom. The study is carried out in lambda (Λ) system, N-system, and modified inverted-Y system (IY^+). Under certain conditions, EIT in Λ-system has been found to be more appropriate for application in tight laser frequency locking and multi-channel optical communications. The signals obtained in N-systems suggest that in this configuration, it is easier to switch from transparency to absorption signal leading to its application in optical switching devices. The IY^+-system is investigated theoretically using a numerical matrix propagation (NMP) method. This study expounds the behavior of the EIT signal in different conditions.

1. EIT in Λ-system

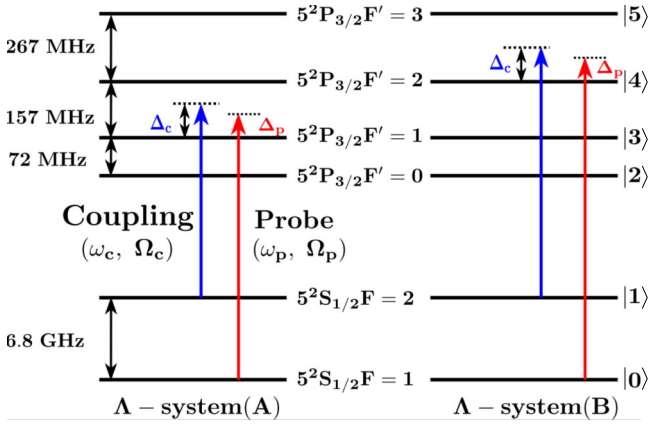

Fig. T.4.1: The two Λ-systems in D_2 line transition of ^{87}Rb atom.

A Λ-system is created using a pump and a probe beam connecting two different ground states with a common excited state of ^{87}Rb atom. Earlier studies on EIT suggest that the Λ-system exhibits minimal coherence dephasing rate of the dipole forbidden transition, which offers higher strength of EIT signal [4]. On that account, a Λ-system has been chosen to begin the investigation of the EIT signal in a vapor cell. In the D_2 line transition of ^{87}Rb atom, there is a possibility of creating two Λ systems (named as system (A) and system (B)), which differ from each other in terms of their coupling transition strength and neighboring excited hyperfine states. These two Λ systems are shown in Figure T.4.1. In the experiment, the probe and pump beams were derived from two different diode lasers.

The two beams were made to co-propagate through the Rb vapor cell. After the vapor cell, the only probe beam is then collected on a photo-diode to get the probe transmitted signal. For Λ-system (A) and (B), probe frequency was kept fixed across transitions $|5^2S_{1/2}\ F=1\rangle \rightarrow |5^2P_{3/2}\ F'=1\rangle$ and $|5^2S_{1/2}\ F=1\rangle \rightarrow |5^2P_{3/2}\ F'=2\rangle$, respectively. The coupling beam's frequency was scanned across the transitions $|5^2S_{1/2}\ F=2\rangle \rightarrow |5^2P_{3/2}\ F'=1, 2, 3\rangle$ for both the Λ systems. The probe signals obtained for the two systems are compared at different conditions, which are discussed in the following sections.

1.1 In the absence of a longitudinal magnetic field

The two Λ-systems are investigated with different power in coupling beam and the observed results are shown in Figure T.4.2.

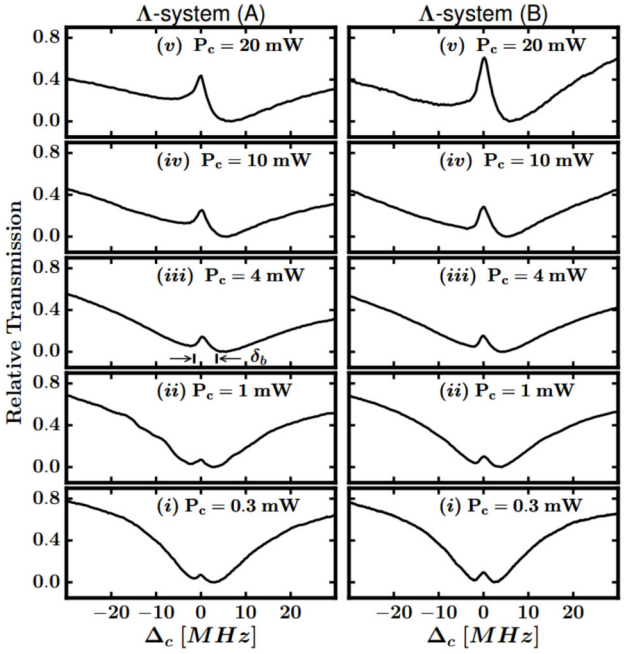

Fig. T.4.2: The probe transmission spectrum in two Λ-systems at different coupling beam power. The probe power is 0.08 mW.

With the increase in coupling beam power, the strength of EIT peak and asymmetry increases in both the systems. On comparing the EIT signal in the two systems, the key features observed are as follows:
i) The system (A) has a more asymmetric line-shape of the EIT signal than that of the system (B). This asymmetry is attributed to the close presence of neighboring excited states in the case of the system (A) [5,6].
ii) The system (B) has shown stronger strength of EIT signal than that in the system (A) for the same coupling power. This is because of the larger dipole matrix element for coupling beam transition in the system (B) as compared to the system (A). Though the line-width of the EIT signal increases as the coupling power increases, even for maximum applied coupling beam power, the line-width of the EIT signal is narrower than the natural line-width of the excited state. Overall, system (B) exhibits a stronger and more symmetric EIT signal than system (A), which evince that system (B) could be a better choice for any EIT application purposes.

1.2 In the presence of a longitudinal magnetic field

On application of a longitudinal magnetic field with respect to the propagation direction of the probe beam, previously obtained single EIT peak splits into three EIT peaks. This is because of splitting of hyperfine levels in Zeeman sub-levels, which results in conversion of a single lambda system into multiple lambda sub-systems. Some of these lambda sub-systems exhibit degenerate two-photon resonance conditions for the occurrence of EIT peak. Thus, in both the lambda systems, we have observed three EIT peaks in presence of a longitudinal magnetic field. The separation between these split-EIT peaks increases with an increase in magnetic field strength. The splitting of a single EIT into three EIT peaks offers an application in multi-channel optical communication.

1.2.1 Characteristics of split EIT peaks with coupling power

This study is carried out by keeping magnetic field strength fixed at 3.4 G and changing the coupling beam power. Figure T.4.3 below shows the observed signal for both the lambda systems with various coupling beam power, where it is evident that separation between peaks is invariant while the strength of the central EIT peak increases with increase in coupling beam power. Also, between two lambda systems, again system (B) exhibits stronger EIT feature than system (A).

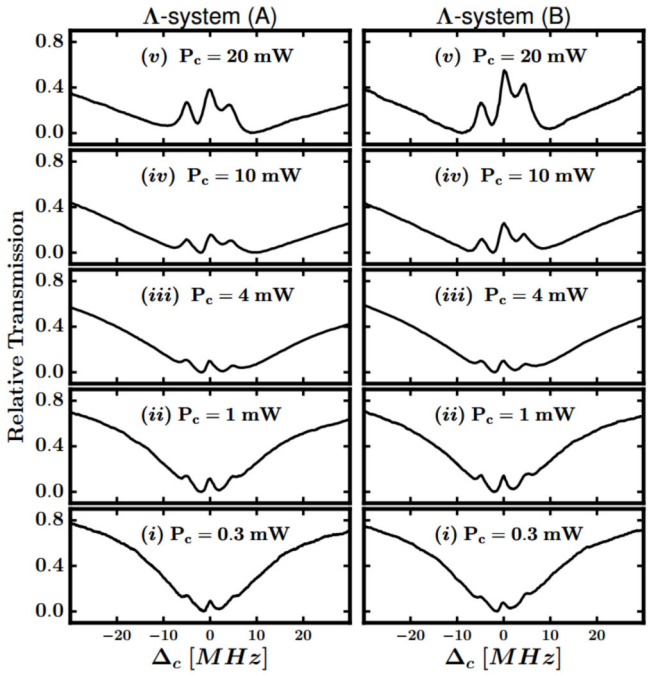

Fig. T.4.3: The probe transmission spectrum in presence of the longitudinal magnetic field at different coupling power for both the Λ-systems.

For coupling beam power greater than 4 mW, the central EIT peak in the presence of the magnetic field has shown larger amplitude and higher slope than the EIT signal in the absence of the magnetic field. For a particular case (Λ-system (B), coupling power = 20 mW, and probe power = 0.08 mW), the slope of the single EIT peak and the central EIT peak in the absence and presence of the magnetic field, respectively are measured and shown in Figure T.4.4.

The slope of the central EIT peak is more than two-fold than the single EIT peak [7]. This suggests that an EIT system with a longitudinal magnetic field can offer an application in laser frequency locking in laboratories.

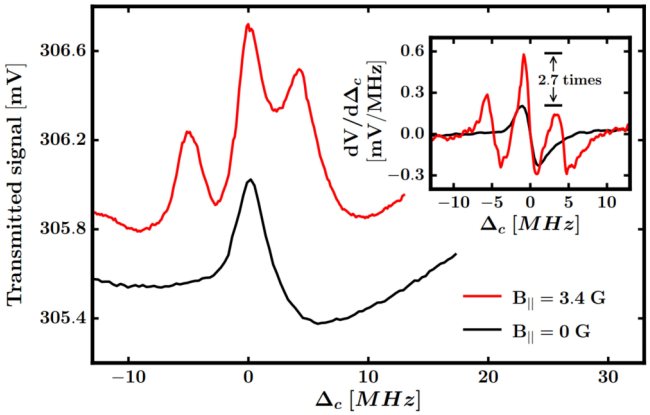

Fig. T.4.4: The probe transmitted signal vs coupling beam detuning. Black and red curves correspond to EIT in the absence and presence of the magnetic field, respectively. Inset shows the slope (derivative with respect to the coupling beam detuning) of the two curves.

1.3 Signal with standing wave coupling field

On obtaining consistently stronger EIT signal for the case of Λ-system (B), further study proceeded with a standing wave coupling field for Λ-system (B) only. At resonance, instead of EIT, an enhanced absorption signal is observed in this case, as shown in Fig T.4.5. This enhanced absorption signal exhibits sub-natural line-width, which suggests that this could be due to the electromagnetically induced absorption (EIA) effect. At higher coupling beam power, the enhanced absorption signal possesses a higher slope with larger magnitude compared to the rest of all the studied cases [8]. This signal is more advantageous than both the EIT cases for precise laser frequency locking application as higher slope means reduced relative frequency uncertainty.

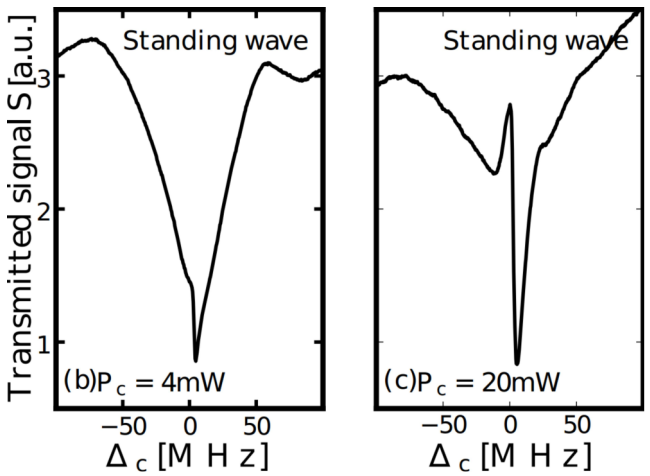

Fig. T.4.5: Probe transmitted signal in presence of a standing wave coupling field for coupling beam powers of 4 mW and 20 mW.

1.4 Theoretical Methods

To model the Λ-systems in the absence and presence of the longitudinal magnetic field, the Hamiltonian under dipole and rotating wave approximation is obtained. In the semi-classical framework, the evolution of the system can be found out from density matrix formalism. From the Liouville equation of motion, a set of time-dependent differential equations of density matrix elements are derived. The diagonal density matrix elements represent population of atoms in the state, whereas, the off-diagonal density matrix elements represent coherence between two states. Under steady-state conditions, the off-diagonal density matrix element, which corresponds to the states connected by the probe field, is calculated numerically to obtain the probe coherence. From this probe coherence, transmission is obtained as a function of coupling field detuning. The calculated results are in qualitative agreement with the observed experimental results.

2. EIT in N-system

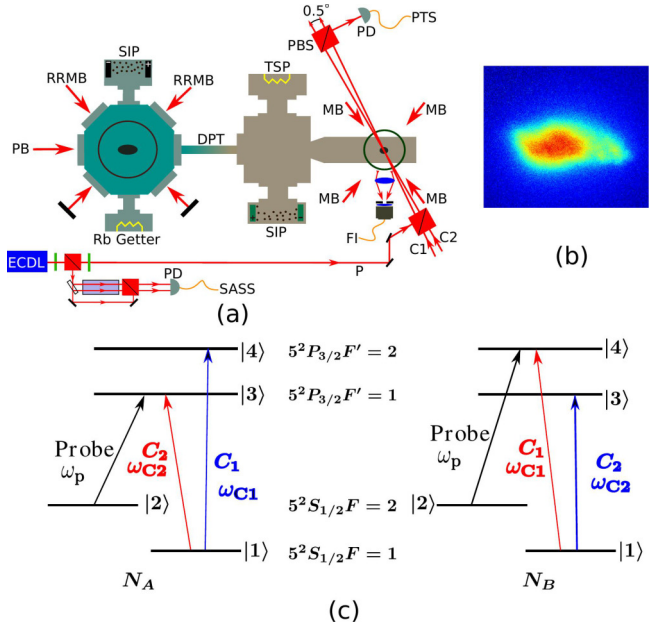

Fig. T.4.6: (a) Schematic diagram of EIT setup in a magneto-optical trap, (b) fluorescence image of ~ 10^7 atoms trapped in MOT, and (c) two N-systems N_A and N_B.

N-system is an extension of Λ-system, where an additional field, named as control field, connects the ground state to another excited state. We created N-system in a magneto-optical trap (MOT), as atoms trapped in MOT effectively reduce the collisional dephasing rate and remove the Doppler effect in the spectral feature. The N-system is prepared using a weak probe beam and two strong drive beams, one named as coupling (which is essential to form Λ-system) and another named as control beam (additional beam to Λ-system). In the experiment, we fixed the frequencies of two drive beams and scanned the frequency of the probe beam. Depending on the transitions interrogated by the probe beam, N-system is referred as N_A ($|2\rangle \rightarrow |3\rangle$) and N_B ($|2\rangle \rightarrow |4\rangle$). The schematic of the experimental setup with fluorescence image of MOT atoms and prepared N-systems are visible in Figure T.4.6.

In experiments, the probe transmission spectrum as a function of probe beam detuning is measured, where three transmission dips for the N-system are observed. The experimentally observed results are backed up with numerical study as well. In the numerical studies, the four-level N-systems are modeled in the same way as described in Section 1.4. A set of differential equations obtained from the Liouville master equation was then solved using the matrix method.

2.1 Effect of coupling and control beam's strength on N-system

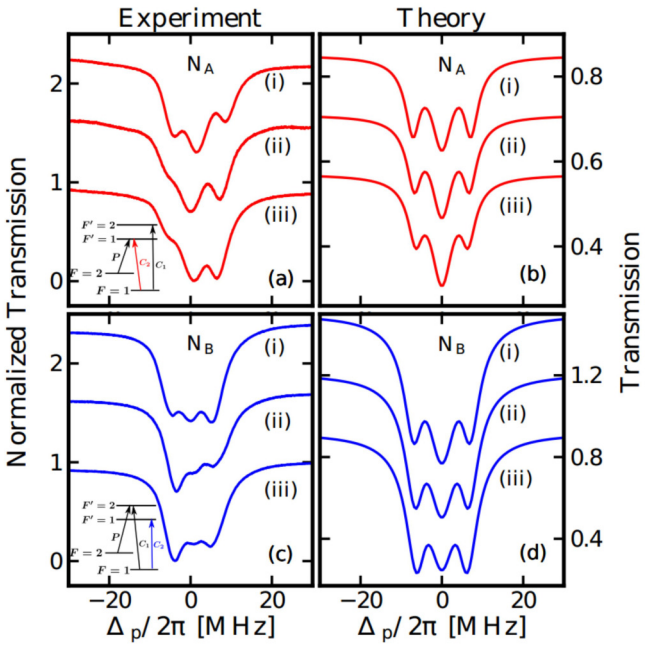

Fig. T.4.7: (a) and (b) show probe transmission spectrum for system N_A obtained experimentally and numerically, respectively, (c) and (d) are for system N_B obtained experimentally and numerically, respectively. Curve (i) is for equal power in both drive beams, i.e., 12 mW; Curve (ii) corresponds to P_{c2} =10 mW; Curve (iii) is for P_{c2} =8 mW. P_{c1} is fixed at 12 mW.

The drive beam C_1 (C_2) acts as a control beam (coupling beam) for system N_A and a coupling beam (control beam) for system N_B. On varying power in beam C_2, while keeping power in beam C_1 fixed, the obtained results can give an insight on the effect of variation in the strength of coupling beam and control beam on N-system by observing the results for system N_A and N_B, respectively.

Figure T.4.7 shows experimentally and numerically obtained signals for different powers in beam C_2. The Figures T.4.7(a) and T.4.7(b) suggest that with decrease in coupling beam power, the strength of side transmission dips also reduces. On the other hand, the Figures T.4.7(c) and T.4.7(d) evince that with decrease in control beam power, the strength of central transmission dip decreases. This implies that in an N-system, two side transmission dips are due to the coupling beam and central transmission dip is due to the control beam.

These three transmission dips can also be understood from the dressed state approach [9]. Two strong drive beams create three dressed states, which on coupling with probe beam from ground states result in three dips in the transmission spectrum (Figure T.4.8).

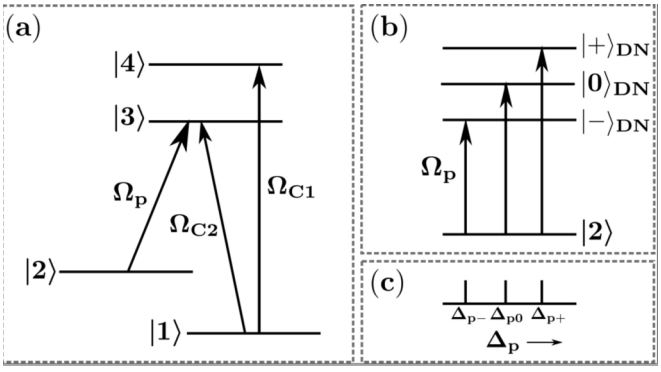

Fig T.4.8. Left side shows the bare state of the N-system. Right side shows corresponding dressed states when Ω_{C1} and Ω_{C2} both are of same strength. The probe transmission from ground state to dressed states result in three dips.

2.2 Effect of coupling and control beam's detuning on N-system

In Figure T.4.9, the experimental and numerical results for two N-systems are shown for the case when frequency of the drive beam C_2 is detuned, while keeping drive beam C_1 frequency fixed at resonance. The power in both the drive beams are 12 mW. For system N_A, detuning of beam C_2 implies detuning of coupling beam. The coupling beam detuning results in asymmetric three transmission dips, which are evident from Figure T.4.9(a) and T.4.9(b). Figures T.4.9(c) and T.4.9(d) show that detuning of the control beam in the N-system leads to asymmetric EIT signal. This is because a detuned control beam converts the N-system into a lambda system with some perturbation. Thus, the absorption signal (three transmission dips) can be converted to transmission signal (two transmission dips) at zero probe detuning by changing the control beam detuning in the N-system. This feature finds its application in optical switching devices.

The studies made on N-systems gave more understanding on the behavior of atomic system interacting with coherent electromagnetic waves [10]. The two drive beams in N-system give more degree of freedom to control and manipulate the spectral features depending on the strength and detuning parameters of the drive beams.

3. Modified inverted-Y system (IY^+-system)

The aim behind the study of IY^+-system is that this system consists of three basic systems (Λ [11], ladder [12] and Vee [13]) and two basic derived systems (inverted-Y and N) that can exhibit EIT feature. By investigating the IY^+-system, an insight on the interdependence of these basic systems can be gained. Along with this, due to the presence of three strong drive fields and one probe field, more control over spectral features can be obtained.

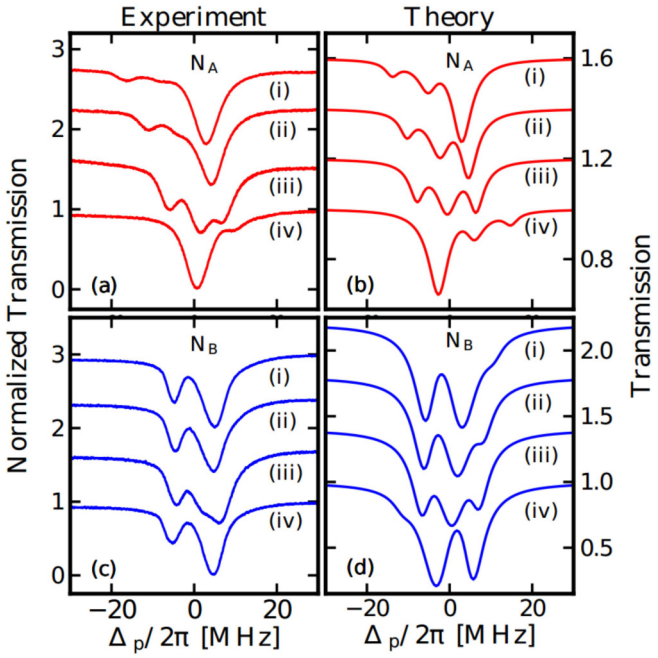

Fig. T.4.9: (a) and (b) show probe transmission spectrum for system N_A obtained experimentally and numerically, respectively, (c) and (d) are for system N_B obtained experimentally and numerically, respectively. Detuning Δ_{C2} in Curve (i) is - 8 MHz, (ii) is - 4 MHz, (iii) is 1 MHz, and (iv) is 9 MHz. Here, $\Delta_{C1}=0$ and $P_{c1}=P_{c2}=12$ mW.

The level diagram of the IY^+-system is shown in Figure T.4.10, where |i> (i ϵ {0,1,2,3,4}) represents atomic states, Ω_{ij} shows the strength of the applied electromagnetic fields, and detuning of the fields are shown by Δ_{ij}. In the Figure T.4.10, |0> ↔ |2> ↔|1> shows Λ-system, |0> ↔ |2> ↔|3> shows ladder system, and |2> ↔ |0> ↔|4> is Vee system. The probe field is represented by strength Ω_{02} and detuning Δ_{02}, whereas the rest of the fields are strong drive fields. The IY^+-system is explored theoretically using a method, named as numerical matrix propagation (NMP) method [14]. In this method, the whole density matrix is propagated in time to achieve the steady state. The NMP method works properly even for the case where rotating wave approximation breaks down. The detail of NMP method is described in [15,16].

The parametric dependence of external parameters on the IY^+-system is discussed in the following subsections.

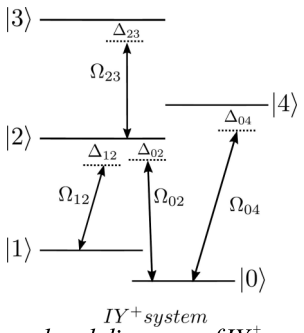

Fig. T.4.10: Energy level diagram of IY^+-system.

3.1 Effect of detuning Δ_{12}

When Δ_{12} is detuned, effectively lambda system within the IY^{+}-system is detuned. This is also evident from Figure T.4.11(b), as Δ_{12} is red detuned, the corresponding red detuned EIT signal is obtained (circled in red color) and so is true for the blue detuned case. When Δ_{12} is zero, there are three absorption peaks. These peaks are explainable from the semi-classical dressed state approach (see Figure T.4.12). The two strong drive beams Ω_{12} and Ω_{23} create three dressed states $|->_1$, $|0>_D$, and $|+>_1$. The drive beam Ω_{04} creates two ground dressed states $|->2$ and $|+>_2$. On calculating the frequency of probe absorption from two ground dressed states to three excited dressed states, we obtained four frequencies. Among these four frequencies, two middle frequencies are very close to each other, which may explain the broadened central peak along with two side peaks for the case of zero Δ_{12} (black curve in Figure T.4.11 (b)).

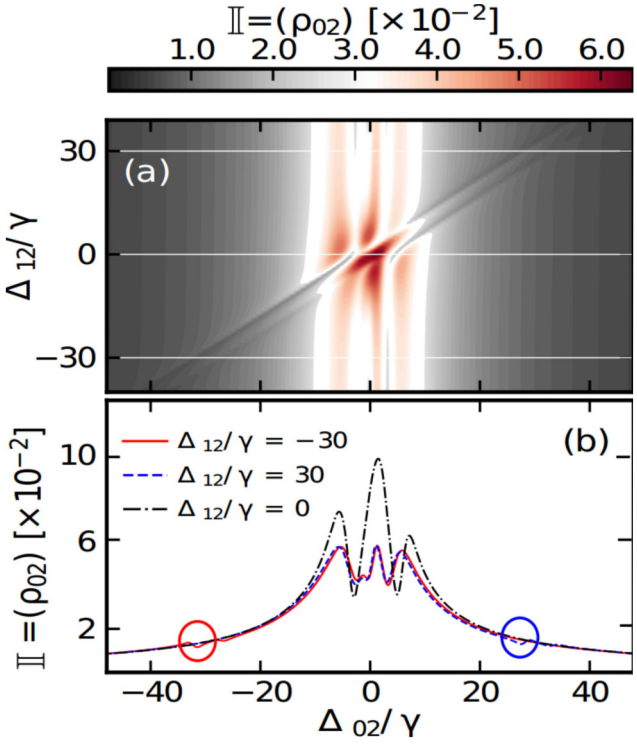

Fig. T.4.11: (a) Shows the calculated probe absorption signal as a function of detuning Δ_{02}, and detuning Δ_{12}, and (b) is the spectrum corresponding to white lines drawn in plot (a).

3.2 Effect of detuning Δ_{04} and Δ_{23}

For further studies, detuning Δ_{12} is kept large, so that its effect can be decoupled from the rest of the external parameters. When detuning Δ_{04} is large and Δ_{23}=0, the four absorption peaks at resonance turn into three absorption peaks with sharp transparencies between them (see Figure T.4.13(a) and T.4.13(b)). The physical explanation for this feature can be given as follows.

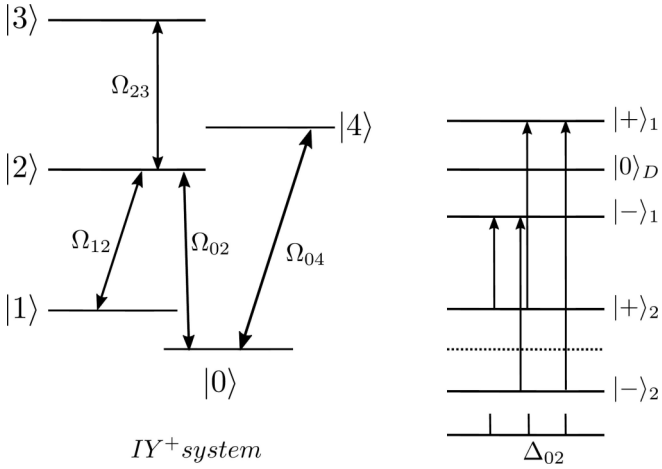

Fig. T.4.12: Left side shows bare state of IY^{+}-system. Right side shows corresponding dressed state. Ω_{12} and Ω_{23} create three excited dressed states and Ω_{04} creates two ground dressed states. The probe absorption from two dressed ground states to three dressed excited states gives three peaks.

For zero detuning Δ_{04}, the emergence of absorption peak at resonance could be the result of constructive quantum interference in the Vee sub-system [17,18]. As the detuning Δ_{04} increases, the effective coupling of this strong field reduces, which consequently reduces the constructive quantum interference effect.

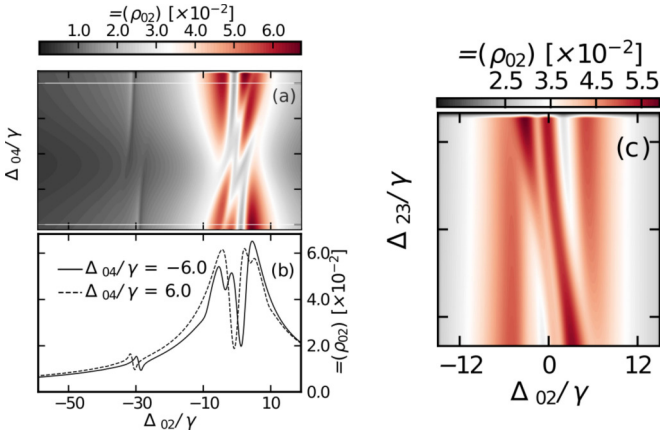

Fig. T.4.13. (a) Shows the calculated probe absorption signal as a function of detuning Δ_{02}, and detuning Δ_{04} when Δ_{23} =0., (b) Individual spectrum corresponding to white lines drawn in plot (a), and(c) shows the calculated probe absorption signal as a function of detuning Δ_{02}, and detuning Δ_{23}, when Δ_{04} =0.

Next, for the case, when Δ_{23} is large and Δ_{04} is zero, the central peak shifts in its position, and another central peak changes its position and strength. Also, a sharp transparency window appears as the detuning Δ_{23} value is increased on either positive or negative side. As the coupling field of the ladder sub-system changes towards the positive side, the transparency shifts in the negative side and vice-versa (see Figure T.4.13(c)).

This manifests that the transparency could be the consequence of destructive quantum interference due to the ladder sub-system.

A similar numerical study is made with the strength of Ω_{12}, Ω_{04}, and Ω_{23}. In strength dependent studies, shifting and splitting of absorption peaks are obtained. These results are explainable using a doubly dressed state approach.

4. Conclusion

This article describes the experimental and theoretical study of EIT in different schemes prepared in D_2 line transition of ^{87}Rb atoms at room temperature and in cold atom cloud trapped in a magneto-optical trap (MOT). On exploration of Λ-systems, the study finds that system (B) could be a better choice for practical applications and signal with standing wave coupling field would be best candidate for tight laser frequency locking application. Studies performed in N-systems and IY$^+$-system provide insight into the responses of these atomic systems to the coherent electromagnetic fields. In these studies, splitting, shifting, and switching of absorption or transparency signals have been obtained, which pave the way for application in multi-channel optical communication and optical switching devices.

Acknowledgements

The work presented in this article is a part of the author's thesis, which was carried out under the mentorship of Dr. S. R. Mishra at LPAS, RRCAT under HBNI program. Author is grateful to Dr. S. R. Mishra for his continuous support, encouragement, and scientific discussions throughout the Ph. D. Author acknowledges Dr. V. B. Tiwari, Dr. S. P. Ram, Dr. S. Singh, Dr. Arijit Chakraborty, Shri Vivek Singh, Shri Sanjeev Tiwari, Smt. Amrita Srivastava and Shri Amit Chaudhary for their help during the experiments. The author is also thankful to Dr. Arup Banerjee for his advice and discussions on the subject. The author's gratitude extends to the Doctoral committee members and Dr. S. Pradhan for their constructive feedback. A special thanks to the previous and current Directors of RRCAT for their support during the work carried out and RRCAT and HBNI for providing the financial support.

References

[1] Melissa A. Guidry, Elena Kuchina, Irina Novikova, and Eugeniy E. Mikhailov. "Characterization of frequency stability in electromagnetically induced transparency-based atomic clocks using a differential detection scheme," J. Opt. Soc. Am. B, 34, 2244, (2017).

[2] Y. B. Kale, S. R. Mishra, V. B. Tiwari, S. Singh, and H. S. Rawat. "Resolution of hyperfine transitions in metastable 83Kr using electromagnetically induced transparency," Phys. Rev. A, 91, 053852, (2015).

[3] S. C. Bell, D. M. Heywood, J. D. White, J. D. Close, and R. E. Scholten, "Laser frequency offset locking using electromagnetically induced transparency," Applied Physics Letters, 90, 171120, (2007).

[4] David J. Fulton, Sara Shepherd, Richard R. Moseley, Bruce D. Sinclair, and Malcolm H. Dunn, "Continuous-wave electromagnetically induced transparency: A comparison of v, Λ, and cascade systems," Phys. Rev. A, 52, 2302, (1995).

[5] Vineet Bharti and Ajay Wasan. "Electromagnetic induced transparency in the doppler broadened cascade transition with multiple excited levels," Journal of Physics B: Atomic, Molecular and Optical Physics, 45, 185501, (2012).

[6] Chen, Zhuo Ren and Su, Xue Mei. "Asymmetrical spectra due to atomic coherence of neighboring excited levels," Eur. Phys. J. D, 67, 138, (2013).

[7] Charu Mishra, A. Chakraborty, A. Srivastava, S. K. Tiwari, S. P. Ram, V. B. Tiwari, S. R. Mishra, "Electromagnetically induced transparency in Λ-systems of 87Rb atom in magnetic field," J. Mod. Opt. 65, 2269, (2018).

[8] Charu Mishra, A. Chakraborty, Vivek Singh, S. P. Ram, V. B. Tiwari, S. R. Mishra, "Coupling field dependent quantum interference effects in a Λ-system of 87Rb atom," Phys. Lett. A, 382, 3269, (2018).

[9] Yong-qing Li and Min Xiao. "Observation of quantum interference between dressed states in an electromagnetically induced transparency," Phys. Rev. A, 51, 4959, (1995).

[10] Charu Mishra, A. Chakraborty, S. P. Ram, S. Singh, V. B. Tiwari, S. R. Mishra, "On electromagnetically induced transparency in N-systems in cold 87Rb atoms," J. Phys. B: At. Mol. Opt. Phys. 53, 015001, (2019).

[11] Yong-qing Li and Min Xiao. "Electromagnetically induced transparency in a three-level Λ-type system in rubidium atoms," Phys. Rev. A, 51, R2703, (1995).

[12] M. Anil Kumar and Suneel Singh. "Electromagnetically induced transparency and slow light in three-level ladder systems: Effect of velocity-changing and dephasing collisions," Phys. Rev. A, 79, 063821, (2009).

[13] Jianming Zhao, Lirong Wang, Liantuan Xiao, Yanting Zhao, Wangbao Yin, and Suotang Jia. "Experimental measurement of absorption and dispersion in v-type cesium atom," Optics Communications, 206, 341, (2002).

[14] Charu Mishra, A. Chakraborty, and S. R. Mishra," Spectral characteristics of a modified inverted-Y system beyond rotating wave approximation" J. Phys. B: At. Mol. Opt. Phys. 52, 095002, (2019).

[15] Masayoshi Nakano and Kizashi Yamaguchi. "Numerical Liouville approach: A calculation method for nonlinear optical susceptibilities of N-state systems," Phys. Rev. A, 50, 2989, (1994).

[16] Masayoshi Nakano and Kizashi Yamaguchi. "Numerical Liouville approach: intensity-dependent transient linear and nonlinear optical susceptibilities," Chemical Physics Letters, 234, 323, (1995).

[17] G S Agarwal, "Nature of the quantum interference in electromagnetic-field-induced control of absorption," Phys. Rev. A 55, 2467, (1997).

[18] C-L Cui, J-K Jia, Y Zhang, Y Xue, H-L Xu, and J-H Wu, "Resonant gain suppression and superluminal group velocity in a multilevel system," J. Phys. B: At. Mol. Opt. Phys. 44, 215504 (2011).